Journal of Science and Technology in Civil Engineering, HUCE (NUCE), 2021, 15 (4): 1–14

# FREE VIBRATION AND DYNAMIC RESPONSE OF SANDWICH COMPOSITE PLATES WITH AUXETIC HONEYCOMB CORE

Tran Huu Quoc[a,*], Tran Minh Tu[a], Vu Van Tham[a]

[a] *Faculty of Building and Industrial Construction, Hanoi University of Civil Engineering, 55 Giai Phong road, Hai Ba Trung district, Hanoi, Vietnam*

***Article history:***
*Received 12/08/2021, Revised 17/09/2021, Accepted 20/09/2021*

**Abstract**

This paper deals with the free vibration and dynamic responses of composite sandwich plates. The sandwich plate has three layers in which two face sheets are made of isotropic material, and the core layer is made of auxetic honeycomb structures with a negative Poisson's ratio. A smoothed finite element model based on the first-order shear deformation theory is established for the analysis purpose. In the model, only the linear approximation is necessary, and the discrete shear gap method for triangular plate elements is used to avoid the shear locking. The Newmark direct integration technique is used to capture the dynamic responses of the sandwich plates. The convergence study is made, and the accuracy of present results is validated by comparison with available data in the literature. The influence of geometrical parameters, material properties, and boundary conditions are explored and discussed. Numerical results show that auxetic materials have several different responses compared to conventional materials, and these behaviors are strongly influenced by the internal structure of the auxetic material.

*Keywords:* dynamic response; sandwich auxetic composite; finite element method; free vibration; honeycomb core.

https://doi.org/10.31814/stce.huce(nuce)2021-15(4)-01 

## 1. Introduction

Sandwich structures possess many outstanding features such as high stiffness to weight ratios, excellent energy absorption, great blast resistance, and very good acoustic and thermal isolation, so they are commonly used in light structural applications. The mechanical properties of sandwich structures on the one side depending on the face sheets materials, but on the other side depending on the chosen core material. Honeycombs with a negative Poisson ratio, named auxetic, have several specific mechanical properties compared to conventional ones, such as high shear modulus, fracture toughness, and indentation resistance. Thus, honeycomb sandwich structures with negative Poisson's ratio are widely used in many areas, including civil aviation, marine, shipbuilding, automobile, civil construction due to their ultra properties such as higher stiffness, lightweight, and high-energy absorption.

There have been several studies and achievements on honeycomb sandwich structures using various theoretical models and computational methods. Scarpa and Tomlinson [1] analyzed the free vibration of the simply supported composite sandwich plates (CSP) with in-plane negative Poisson's

*Corresponding author. *E-mail address:* quocth@nuce.edu.vn (Quoc, T. H.)

ratio based on the first-order shear deformation plate theory (FSDT). Hadjigeorgiou and Stavroulakis [2] proposed a sandwich beam model with piezoelectric face sheets and auxetic core for shape control based on Timoshenko beam theory and finite element method (FEM). Ruzzene et al. [3] analyzed and controlled wave propagation in CSP with the cellular core by using Kirchhoff plate theory and FEM. Strek and co-workers [4] used a finite element model to study the effective properties and dynamic response of the sandwich panel with an auxetic core layer. Mukhopadhyay and Adhikari [5] developed a closed-form formula to study how random structural irregularity in honeycomb core affects the natural frequencies of sandwich panels. Imbalzano et al. [6] investigated the blast resistance of sandwich panels composed of the auxetic cellular core. The buckling behaviors of a rectangular auxetic material plate under uniaxial compression were reported by Yongcun and his colleagues [7]. Duc et al. [8] presented an analytical solution based on the FSDT and Galerkin method for nonlinear vibration and dynamic analysis of cylindrical panels made by auxetic honeycomb composite sandwich material. Using LS-DYNA, Novak et al. [9] built the computational model to validate experimental results in studying blast respose of sandwich panels with chiral auxetic core. Cong et al. [10] analyzed the nonlinear dynamic response of stiffened sandwich circular shells with auxetic honeycombs core sourounded by elastic medium under mechanical and blast loads. Postbuckling analysis of CSP with FG auxetic 3D lattice core subjected to thermomechanical loads has been introduce ted by Li et al. [11]. Employing the classical plate theory inconjjunction with Galerkin method, Quan et al. [12] presented nonlinear dynamic and vibaritional characteristics of CSP composed of gold and piezoelectric face sheets, and auxetic honeycomb core. Nguyen et al. [13] investigated vibrational characteristics, buckling behavior and dynamic instability of CSP consist of auxetic honeycomb core and face sheets reinforced by graphene nanoplatelets that have been instigated by using polygonal plate element and are reported.

With the development of new materials and their application in different engineering structures, many computational models have been developed to predict these structures' responses. For the plates and shell, the models are based on the displacement-based theories, which can be classified into three categories: classical plate theory (CPT), first-order shear deformation theory (FSDT), and higher-order shear deformation theory (HSDT). While the models based on the CPT [14] are simple but only provides accurate results for thin plates and shells, the models based on HSDT [15–18] are so complicated, the models based on FSDT [19, 20] can be used for both thin and thick plates and shells. However, models based on FSDT often suffer from two major drawbacks; (1) the "shear locking"phenomena, which pollute the numerical results in the thin limit, and (2) the overly stiff behavior, which leads to poor accuracy and low convergence of numerical solutions. To avoid these problems of the FSDT model, a smooth finite element model, so-called the cell-based smoothed discrete shear gap method (CS-DSG3) using the cell-based strain smoothing technique and three-node triangular elements, has been developed by T Nguyen-Thoi et al. [21]. In the CS-DGS3 model, the strain components of each triangle element are calculated through the strain components of three sub-triangles, so the calculation time of the CS-DSG3 model will be more than that of the flat element model.

It can be seen that to avoid the shear locking phenomenon when using FSDT, a smooth finite element method with more computation time than conventional FEM can be used. However, to evaluate the efficiency of this combination as well as to enrich the computational models, in this paper, a sandwich plate with auxetic honeycomb core layer (AHCL) and isotropic face sheets is chosen to study. Free vibration and dynamic response analysis of auxetic composite sandwich plates are analyzed. After some comparative examples for validating the model, a few new investigations about the influence of material properties, geometrical parameters, and boundary conditions on vibrational characteristics of the auxetic sandwich composite plates are conducted.

## 2. Sandwich composite plate with auxetic core

### 2.1. Description of the problem

A rectangular sandwich plate with length $a$, width $b$, and total thickness $h_p$, as shown in Fig. 1, is considered in this study. The thicknesses of the bottom, core, and top layers are $h_1, h_2$, and $h_3$, respectively. The top and bottom outer skin layers are made of isotropic aluminum materials, while the core is made of an auxetic honeycomb structure using the same aluminum material.

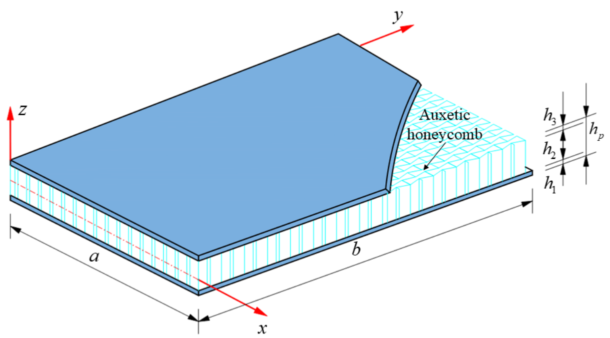


Figure 1. Model of an AHCL sandwich plate

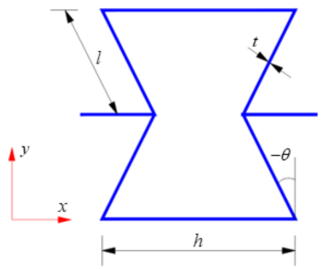


Figure 2. Unit cell layout for the honeycomb structure

### 2.2. Auxetic honeycomb materials

The mechanical properties of a honeycomb unit cell depend not only on the original material properties but also on the vertical cell rib length $h$, the inclined cell rib length $l$, and the inclined angle $\theta$.

The material properties of the AHCL are given by [22]:

$$\begin{aligned}
&E_1^C = E\left(\frac{t}{l}\right)^3 \frac{\cos\theta}{(h/l+\sin\theta)\sin^2\theta}; \quad E_2^C = E\left(\frac{t}{l}\right)^3 \frac{(h/l+\sin\theta)}{cos^3\theta} \\
&\upsilon_{12}^C = \frac{\cos^2\theta}{\left(\frac{h}{l}+\sin\theta\right)\sin\theta}; \quad \upsilon_{21}^C = \upsilon_{12}^C \\
&G_{12}^C = E\left(\frac{t}{l}\right)^3 \frac{\left(\frac{h}{l}+\sin\theta\right)}{\left(\frac{t}{l}\right)^3\left(1+2\frac{h}{l}\right)\cos\theta}; \quad G_{13}^C = G\left(\frac{t}{l}\right)\frac{\cos\theta}{\frac{h}{l}+\sin\theta} \\
&G_{12}^C = E\left(\frac{t}{l}\right)^3 \frac{\left(\frac{h}{l}+\sin\theta\right)}{\left(\frac{h}{l}\right)^3\left(1+2\frac{h}{l}\right)cos\theta}; \quad G_{13}^C = G\frac{t}{l}\frac{\cos\theta}{\frac{h}{l}+\sin\theta} \\
&G_{23}^C = G\frac{t}{l}\frac{1+2\sin^2\theta}{2\cos\theta\left(\frac{h}{l}+\sin\theta\right)}; \quad \rho^C = \rho\frac{\frac{t}{l}\left(\frac{h}{l}+2\right)}{2\cos\theta\left(\frac{h}{l}+\sin\theta\right)}
\end{aligned} \tag{1}$$

where $E, G$, and $\rho$ are Young's moduli, shear moduli, and mass density of the original material; subscript symbol "$C$" refers to the core layer.

## 3. Formulations

### *3.1. Equations of motion for plate element*

According to FSDT, the displacement field is defined as

$$\begin{aligned} u(x,y,z,t) &= u_0(x,y,t) + z\theta_x(x,y,t) \\ v(x,y,z,t) &= v_0(x,y,t) + z\theta_y(x,y,t) \\ w(x,y,z,t) &= w_0(x,y,t) \end{aligned} \tag{2}$$

where $t$ is the time; $u_0$, $v_0$, and $w_0$ are displacements of a point at the mid-plane; $\theta_x$ and $\theta_y$ are rotations of the transverse normal in $yz$ and $xz$ planes, respectively. The strain fields can be written as follows

$$\begin{aligned} &\left\{ \begin{array}{c} \varepsilon_{xx} \\ \varepsilon_{yy} \\ \gamma_{xy} \end{array} \right\} = \left\{ \begin{array}{c} u_{0,x} \\ v_{0,y} \\ u_{0,y} + v_{0,x} \end{array} \right\} + z \left\{ \begin{array}{c} \theta_{x,x} \\ \theta_{y,y} \\ \theta_{x,y} + \theta_{y,x} \end{array} \right\} = \varepsilon^m + z\kappa \\ &\left\{ \begin{array}{c} \gamma_{xz} \\ \gamma_{yz} \end{array} \right\} = \left\{ \begin{array}{c} \theta_x + w_{0,x} \\ \theta_y + w_{0,y} \end{array} \right\} = \gamma \end{aligned} \tag{3}$$

where $\varepsilon^m$, $\kappa$ and $\gamma$ are membrane, bending, and shear strains, respectively; the subscript "comma" represents the partial derivative to the spatial coordinate succeeding it.

Hooke's law for the AHCL sandwich plates is defined as follows:

$$\left\{ \begin{array}{c} \sigma_x^i \\ \sigma_y^i \\ \tau_{xy}^i \end{array} \right\} = \left[ \begin{array}{ccc} Q_{11}^i & Q_{12}^i & 0 \\ Q_{12}^i & Q_{22}^i & 0 \\ 0 & 0 & Q_{66}^i \end{array} \right] \left\{ \begin{array}{c} \varepsilon_x \\ \varepsilon_y \\ \gamma_{xy} \end{array} \right\}, \qquad (i = T, B, C) \tag{4a}$$

$$\left\{ \begin{array}{c} \tau_{yz}^i \\ \tau_{xz}^i \end{array} \right\} = \left[ \begin{array}{cc} Q_{44}^i & 0 \\ 0 & Q_{55}^i \end{array} \right] \left\{ \begin{array}{c} \gamma_{yz} \\ \gamma_{xz} \end{array} \right\}, \qquad (i = T, B, C) \tag{4b}$$

where

$$\begin{aligned} &Q_{11}^C = \frac{E_1^C}{1 - \nu_{12}^C \nu_{21}^C};\ Q_{12}^C = \frac{\nu_{12}^C E_2^C}{1 - \nu_{12}^C \nu_{21}^C};\ Q_{22}^C = \frac{E_2^C}{1 - \nu_{12}^C \nu_{21}^C};\ Q_{44}^C = G_{23}^C;\ Q_{55}^C = G_{12}^C;\ Q_{66}^C = G_{12}^C \\ &Q_{11}^i = \frac{E^i}{1 - \nu_i^2}; \quad Q_{12}^i = \frac{\nu_{12}^i E^i}{1 - \nu_i^2}; \quad Q_{22}^i = Q_{11}^i; \quad (i = T, B) \\ &Q_{44}^i = G_{23}^i; \quad Q_{55}^i = G_{12}^i; \quad Q_{66}^i = G_{12}^i; \quad (i = T, B) \end{aligned} \tag{5}$$

In Eq. (4) and (5), "$T$", "$B$", and "$C$" refer to the top, bottom, and core layers. Applying Hamilton's principle, the equations of motion are derived by:

$$\delta \int_{t_0}^{t_1} [T - (U + W)]\, dt = 0 \tag{6}$$

where $\delta$ is the notation of variation, $W$ is the external work. Meanwhile, $T$ is the kinetic energy, and $U$ is the strain energy of the plate.

The strain energy of the plates is determined as follows

$$U = \frac{1}{2}\int_V \left(\sigma_{xx}\varepsilon_{xx} + \sigma_{yy}\varepsilon_{yy} + \sigma_{xy}\gamma_{xy} + \tau_{xz}\gamma_z + \tau_{yz}\gamma_{yz}\right) dV$$
$$= \frac{1}{2}\int_0^b\int_0^a \left\{ \begin{array}{ccc} (\varepsilon^m)^T & \kappa^T & \gamma^T \end{array} \right\} \left[ \begin{array}{ccc} A & B & 0 \\ B & D & 0 \\ 0 & 0 & D_s \end{array} \right] \left\{ \begin{array}{c} \varepsilon^m \\ \kappa \\ \gamma \end{array} \right\} dxdy \tag{7}$$

where

$$(A, B, D) = \int_{-\frac{h_2}{2}-h_1}^{-\frac{h_2}{2}} Q_{ij}^B\left(1, z, z^2\right) dz + \int_{-\frac{h_2}{2}}^{\frac{h_2}{2}} Q_{ij}^C\left(1, z, z^2\right) dz + \int_{\frac{h_2}{2}}^{\frac{h_2}{2}+h_3} Q_{ij}^T\left(1, z, z^2\right) dz, \quad i = 1, 2, 6 \tag{8}$$

$$D_s = \int_{-\frac{h_2}{2}-h_1}^{-\frac{h_2}{2}} k_s Q_{ij}^B dz + \int_{-\frac{h_2}{2}}^{\frac{h_2}{2}} k_s Q_{ij}^C dz + \int_{\frac{h_2}{2}}^{\frac{h_2}{2}+h_3} k_s Q_{ij}^T dz, \quad i = 4, 5 \tag{9}$$

in which $k_s = \dfrac{5}{6}$ is the shear correction factor.

The kinetic energy of the plate is expressed as

$$T = \frac{1}{2}\int_V \left[(\dot{u})^2 + (\dot{v})^2 + (\dot{w})^2\right] dV = \frac{1}{2}\int_0^b\int_0^a (\dot{u})^T m\dot{u}dxdy \tag{10}$$

where

$$m = \left[ \begin{array}{ccccc} I_0 & 0 & 0 & I_1 & 0 \\ 0 & I_0 & 0 & 0 & I_1 \\ 0 & 0 & I_0 & 0 & 0 \\ I_1 & 0 & 0 & I_2 & 0 \\ 0 & I_1 & 0 & 0 & I_2 \end{array} \right] \tag{11}$$

in which

$$(I_0, I_1, I_2) = \int_{-\frac{h_2}{2}-h_1}^{-\frac{h_2}{2}} \rho^B(1, z, z^2)dz + \int_{-\frac{h_2}{2}}^{\frac{h_2}{2}} \rho^C(1, z, z^2)dz + \int_{\frac{h_2}{2}}^{\frac{h_2}{2}+h_3} \rho^T(1, z, z^2)dz \tag{12}$$

The external work due to uniform transverse pressure loading $q$ is given as

$$W = \int_0^b\int_0^a u^T q dxdy \tag{13}$$

### 3.2. CS-DGS3 Finite Element Model

The domain $\Omega$ of the plate is discretized into Ne triangular elements with Nn number of nodes. Each triangular element $\Omega_e$, as shown in Fig. 3, is divided into three sub-triangles $\Delta_1, \Delta_2$ and $\Delta_3$. The displacement vector $d_O^e = \left\{u_{0O}^e, v_{0O}^e, w_{0O}^e, \theta_{xO}^e, \theta_{yO}^e\right\}^T$ of the connecting point O is assumed to be the simple average of three displacement vectors $d_i^e = \left\{u_{0i}, v_{0i}, w_{0i}, \theta_{xi}, \theta_{yi}\right\}^T, (i = 1, 2, 3)$ of three nodes as,

$$d_O^e = \frac{1}{3}\left(d_1^e + d_2^e + d_3^e\right) \tag{14}$$

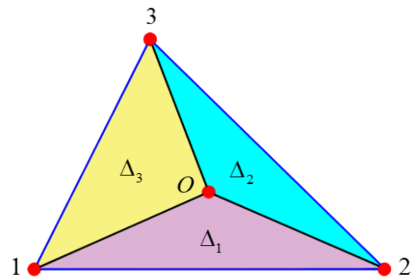


Figure 3. Three sub-triangular ($\Delta_1, \Delta_2$ and $\Delta_3$)

By using the DGS3 formulation and Eq. (14), the membrane, bending, and shear strains in the sub-triangle $\Delta_1$ can be expressed as

$$\varepsilon_m^{\Delta_1} = \underbrace{\left[\begin{array}{ccc} \frac{1}{3}b_{m_1}^{\Delta_1} + b_{m_2}^{\Delta_1} & \frac{1}{3}b_{m_1}^{\Delta_1} + b_{m_3}^{\Delta_1} & \frac{1}{3}b_{m_1}^{\Delta_1} \end{array}\right]}_{B_m^{\Delta_1}} \left\{\begin{array}{c} d_{e_1} \\ d_{e_2} \\ d_{e_3} \end{array}\right\} = B_m^{\Delta_1} d_e \tag{15}$$

$$\kappa_b^{\Delta_1} = \underbrace{\left[\begin{array}{ccc} \frac{1}{3}b_{b_1}^{\Delta_1} + b_{b_2}^{\Delta_1} & \frac{1}{3}b_{b_1}^{\Delta_1} + b_{b_3}^{\Delta_1} & \frac{1}{3}b_{b_1}^{\Delta_1} \end{array}\right]}_{B_b^{\Delta_1}} \left\{\begin{array}{c} d_{e_1} \\ d_{e_2} \\ d_{e_3} \end{array}\right\} = B_b^{\Delta_1} d_e \tag{16}$$

$$\gamma_s^{\Delta_1} = \underbrace{\left[\begin{array}{ccc} \frac{1}{3}S_1^{\Delta_1} + S_2^{\Delta_1} & \frac{1}{3}S_1^{\Delta_1} + S_3^{\Delta_1} & \frac{1}{3}S_1^{\Delta_1} \end{array}\right]}_{S^{\Delta_1}} \left\{\begin{array}{c} d_{e_1} \\ d_{e_2} \\ d_{e_3} \end{array}\right\} = S^{\Delta_1} d_e \tag{17}$$

where $b_{m_i}^{\Delta_1}, b_{b_i}^{\Delta_1}$ and $S_i^{\Delta_1} (i = 1, 2, 3)$ are determined similarly as the strain gradient matrices $b_{m_i}, b_{b_i}$ and $S_i$ of the flat element DSG3 [21]. The cyclic permutation easily obtains the membrane, bending, and shear strains for the second sub-triangle $\Delta_2$ and third $\Delta_3$, respectively.

The smoothed membrane, bending, and shear strain $(\bar{\varepsilon}_m, \bar{\kappa}_b, \bar{\gamma}_s)$ on the triangular element $\Omega_e$ can be obtained by applying the corresponding cell-based formulas.

$$\bar{\varepsilon}_m = \bar{B}_m d_e; \quad \bar{\kappa}_b = \bar{B}_b d_e; \quad \bar{\gamma}_s = \bar{S} d_e \tag{18}$$

where $\bar{B}_m$, $\bar{B}_b$ and $\bar{S}$ are the smoothed membrane, bending and shear gradient matrices, and given by

$$\bar{B}_m = \frac{1}{A_e}\sum_{i=1}^{3} A_{\Delta_i} B_m^{\Delta_i}; \quad \bar{B}_b = \frac{1}{A_e}\sum_{i=1}^{3} A_{\Delta_i} B_b^{\Delta_i}; \quad \bar{S} = \frac{1}{A_e}\sum_{i=1}^{3} A_{\Delta_i} S^{\Delta_i} \tag{19}$$

The equilibrium equation for dynamic analysis of the sandwich plate is obtained by substituting Eq. (18) into Eq. (7), then substituting the results to Eq. (6) and using some mathematical calculations:

$$\mathbf{M}\ddot{\mathbf{d}} + \mathbf{K}\mathbf{d} = \mathbf{F} \tag{20}$$

In Eq. (20), $\mathbf{d}$ and $\ddot{\mathbf{d}}$ are, respectively, the nodal displacement vector and the second-order derivative of displacement, while $\mathbf{K}$, $\mathbf{M}$ and $\mathbf{F}$ are the global stiffness matrix, global mass matrix and global nodal force vector which are assembled from elemental stiffness matrices, elemental mass matrices and elemental nodal force vectors as follow

$$\mathbf{K} = \sum_{i=1}^{N_e} \mathbf{K}_e^{CS-DSG3}; \quad \mathbf{M} = \sum_{i=1}^{N_e} \mathbf{M}_e; \quad \mathbf{F} = \sum_{i=1}^{N_e} \mathbf{F}_e \tag{21}$$

in which

$$\mathbf{K}_e^{CS-DSG3} = \int_{\Omega_e} \left[ \bar{B}_m^T A \bar{B}_m + \bar{B}_m^T B \bar{B}_b + \bar{B}_b^T B \bar{B}_m + \bar{B}_b^T D \bar{B}_b + \bar{S}^T D_s \bar{S} \right] d\Omega \tag{22}$$

$$\mathbf{M}_e = \int_{\Omega_e} \mathbf{N}^T \mathbf{m} \mathbf{N} d\Omega \tag{23}$$

$$\mathbf{F}_e = \int_{\Omega_e} \mathbf{N}^T \mathbf{q} d\Omega \tag{24}$$

where $\mathbf{N}$ is the shape function matrix.

For free vibration analysis, the equation is given as

$$\mathbf{M}\ddot{\mathbf{d}} + \mathbf{K}\mathbf{d} = \mathbf{0} \tag{25}$$

## 4. Numerical results

### *4.1. Validation and Convergence study*

Before proceeding with the parametric studies, convergency and comparison studies are conducted first.

In the first comparison, the fundamental frequencies of a simply supported sandwich plate are computed and compared with those reported by Tran et al. [23] using plate elements within the framework of the finite element method and FSDT. The results are presented in Table 1. The square plate has length $a = b = 2$ m, thickness $h_p = h_2 + h_1 + h_3 = a/20$. The plate has three-layer, the top and bottom layers have thickness $h1 = h3 = hf$, the core has thickness $h_c = h_2 = 1.5h_f$. All layers have the same material properties: $E = 69$ GPa, $\rho = 2700$ kg/m$^3$, and $\upsilon = 0.33$. It can be seen from Table 1 that with the mesh 12×12×2 elements, the obtained results show good agreement with solutions by Tran et al. [23]. So this meshing will be used throughout the numerical examples.

In the following example, the dimensionless central deflection $\bar{w} = \dfrac{wEh_p}{q_0 a^2}$ as functions of dimensionless time $\bar{t} = t\sqrt{E/(a^2\rho)}$ for an isotropic square plate subjected to a suddenly applied uniform load with $q_0 = -10^6$ N/m$^2$ is plotted and compared with those of Reddy [24] as seen in Fig. 4. From this figure can be observed that present results well match with Reddy's report [24], in which the finite element method and third-order shear deformation theory are used.

Table 1. Comparison of fundamental frequency $f$ (Hz) of the AHCL sandwich plate ($h_p$ = 0.1 m, $a = b = 20h_p, t/l = 0.1385$)

| $\theta^\circ$ | Mesh | $h/l = 0.5$ | | $h/l = 1$ | | $h/l = 4$ | |
|---|---|---|---|---|---|---|---|
| | | Present | [23] | Present | [23] | Present | [23] |
| $\theta^\circ = -10^\circ$ | 6×6 | 158.280 | 150.087 | 159.877 | 151.609 | 160.460 | 152.407 |
| | 8×8 | 153.598 | | 155.147 | | 155.712 | |
| | 10×10 | 151.348 | | 152.872 | | 153.428 | |
| | 12×12 | 150.040 | | 151.549 | | 152.340 | |
| $\theta^\circ = -35^\circ$ | 6×6 | 181.633 | 172.323 | 157.957 | 149.783 | 159.976 | 152.196 |
| | 8×8 | 176.247 | | 153.284 | | 155.243 | |
| | 10×10 | 173.637 | | 151.039 | | 152.966 | |
| | 12×12 | 172.111 | | 149.734 | | 152.129 | |
| $\theta^\circ = -55^\circ$ | 6×6 | 167.264 | 158.642 | 150.678 | 142.858 | 158.989 | 151.753 |
| | 8×8 | 162.311 | | 146.223 | | 154.285 | |
| | 10×10 | 159.923 | | 144.087 | | 152.023 | |
| | 12×12 | 158.531 | | 142.848 | | 151.687 | |
| $\theta^\circ = -80^\circ$ | 6×6 | 175.079 | 166.087 | 62.185 | 58.716 | 152.765 | 148.721 |
| | 8×8 | 169.891 | | 60.283 | | 148.247 | |
| | 10×10 | 167.380 | | 59.432 | | 146.077 | |
| | 12×12 | 165.915 | | 58.959 | | 148.661 | |

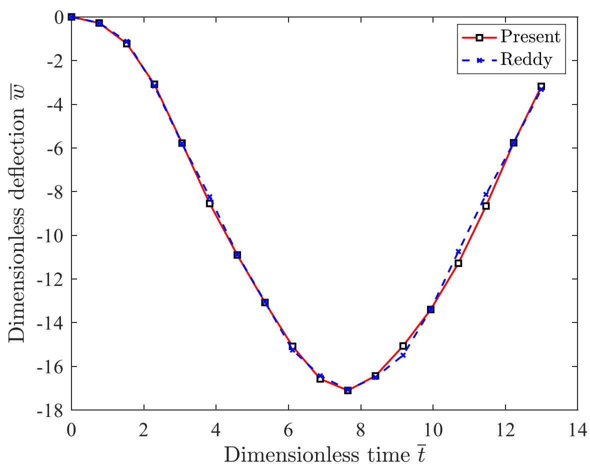


Figure 4. Dimensionless central deflection versus dimensionless time curves for an isotropic square plate subjected to a suddenly applied uniform load

### 4.2. *Parametric studies*

Consider a square plate with thickness $h_p$ = 0.1 m, length $a = b = 20h_p$. The plate has three layers, in which the upper and lower layer are isotropic material, while the core layer is auxetic honeycomb material. Material properties are taken as $E$ = 69 GPa, $\rho$ = 2700 kg/m$^3$, and $\nu$ = 0.33. It is noted that the symbols C, F, and P denote the clamped, free, and pinned boundary conditions, respectively.

a. Free vibration of the ACL sandwich plate

Table 2 lists three first natural frequencies $f$ (Hz) of the AHCL sandwich plate with $t/l = 0.1385$ for various boundary conditions (BC) and different values of inclined angle $\theta$. It is seen that with the investigated BC herein, the CCCC plate has the highest value of fundamental frequency while the CFFF plate has lowes one. This observation is due to the existence of more boundary constraints in the CCCC condition, which results in higher stiffness of the plates. In this specific example, the second and the third natural frequencies of the SSSS and CCCC plates are similar. This phenomenon is suitable for the symmetrical plate structures under the same boundary. It is also observed that the natural frequencies of the AHCL sandwich plate decrease corresponding to the change of the inclined angle from −100 to −800.

Table 2. Three first natural frequency $f$ (Hz) of square AHCL sandwich plate ($h_p = 0.1$ m, $a = b = 20h_p$, $t/l = 0.1385$)

| $\theta^\circ$ | Mode | BCs | | | | | | |
|---|---|---|---|---|---|---|---|---|
| | | CCCC | CSCS | CCCF | SSSS | SCSF | CFCF | CFFF |
| −10° | 1 | 276.812 | 222.493 | 183.101 | 151.549 | 96.480 | 170.143 | 26.700 |
| | 2 | 560.900 | 424.146 | 305.219 | 381.103 | 251.389 | 200.900 | 64.020 |
| | 3 | 570.638 | 534.165 | 485.253 | 384.432 | 322.234 | 330.736 | 162.277 |
| −35° | 1 | 273.555 | 219.835 | 180.901 | 149.734 | 95.317 | 168.091 | 26.373 |
| | 2 | 554.523 | 419.200 | 301.638 | 376.621 | 248.441 | 198.500 | 63.246 |
| | 3 | 564.157 | 527.940 | 479.567 | 379.912 | 318.390 | 326.858 | 160.323 |
| −55° | 1 | 261.191 | 209.682 | 172.500 | 142.848 | 90.911 | 160.253 | 25.135 |
| | 2 | 530.212 | 400.403 | 288.000 | 359.591 | 237.295 | 189.322 | 60.305 |
| | 3 | 539.565 | 503.895 | 457.613 | 362.763 | 303.730 | 312.036 | 152.880 |
| −80° | 1 | 108.599 | 86.324 | 70.787 | 58.959 | 37.417 | 65.599 | 10.268 |
| | 2 | 221.938 | 167.253 | 119.884 | 149.021 | 99.017 | 77.937 | 24.771 |
| | 3 | 229.777 | 208.464 | 188.723 | 151.263 | 125.066 | 129.850 | 62.712 |

Fig. 5 shows the variation of the natural frequencies $f$ (Hz) with the inclined angle $\theta$ (°) at various $h/l$ ratios for the AHCL sandwich plate with SSSS condition (a), with CCCC condition (b), with SCSF condition (c), and with CFFF condition (d). From the figures, it can be observed that the fundamental frequencies for the cases of $h/l = 1$, $h/l = 1.4$, and $h/l = 4$ increase with the decreased inclined angle $\theta$ while those for the case of $h/l = 0.5$ do not follow any rule. Thus, in most cases, cell ribs with smaller incline angles will have a small "grown-together" region around their connecting end, which will make the microstructure stiffer.

Fig. 6 shows the natural frequencies $f$ (Hz) variation with the thickness ratio $h_c/h_f$ at various inclined angles $\theta$. The figure indicates that, unlike conventional materials, auxetic materials with negative Poisson coefficients have very unpredictable vibrational behavior. The free vibration behavior of the AHCL sandwich plate can only be determined for a given set of input parameters. For example, in the case of $h/l = 0.5$, the frequencies of the plate with $\theta = -35^\circ$ are highest and increase rapidly with the thickness ratios hc/hf while the frequencies of the plate with other values of the inclined angle $\theta$ slightly increase. Especially in the case of $h/l = 1.0$, the frequencies of the plate with $\theta = -85^\circ$ are decreased while others increase with the thickness ratios $h_c/h_f$.

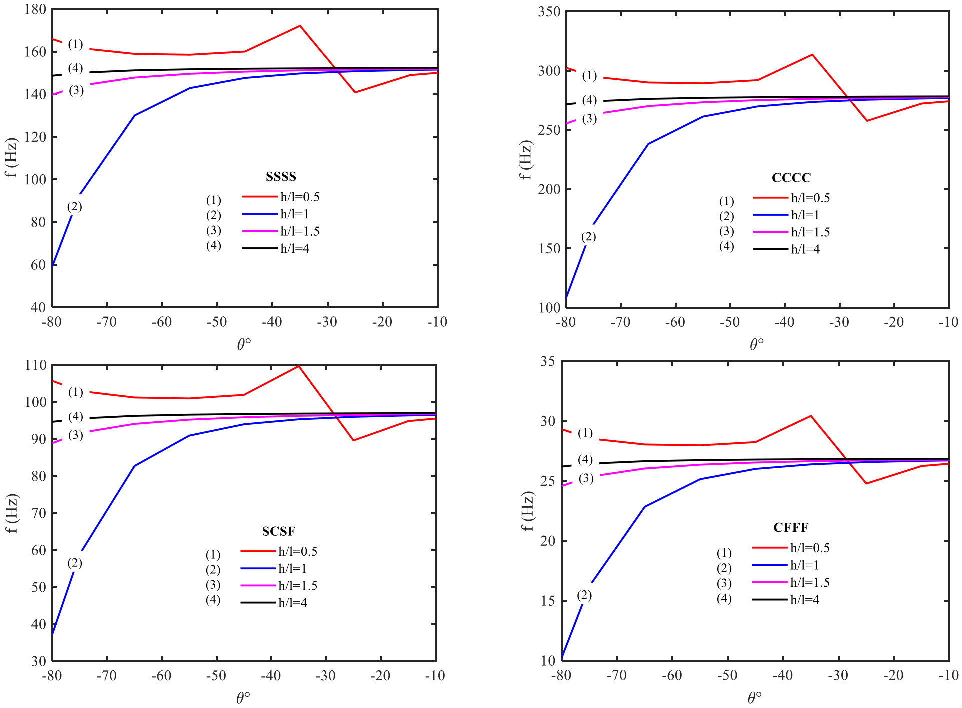


Figure 5. Variations of fundamental frequency $f$ (Hz) with the inclined angle $\theta$ ($h_p = 0.1$ m, $h_c/h_f = 1.5, a = b = 20h_p, t/l = 0.1385$)

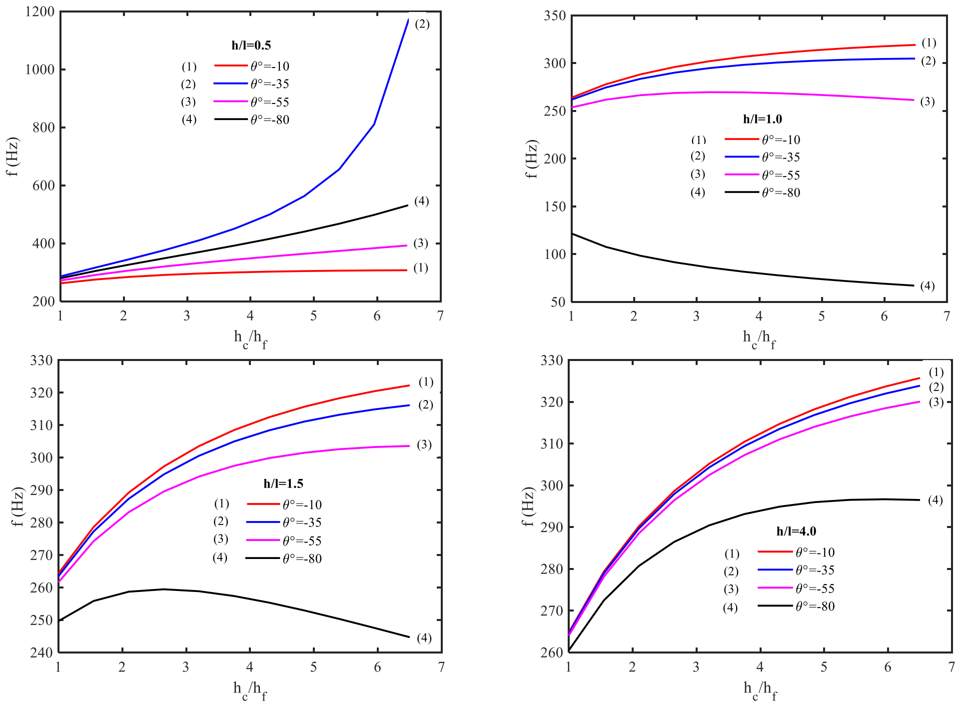


Figure 6. Variations of fundamental frequency $f$ (Hz) with the thickness ratio $h_c/h_f$ ($h_p = 0.1$ m, CCCC, $a = b = 20h_p$, $t/l = 0.1385$)

When the core layer of the SCP is made of auxetic honeycomb material with a negative Poisson ratio, the influence of the ratio between the length of the vertical cell rib and the length of the inclined cell rib $h/l$ should be considered since it is one of the most important geometrical parameters of an auxetic material.

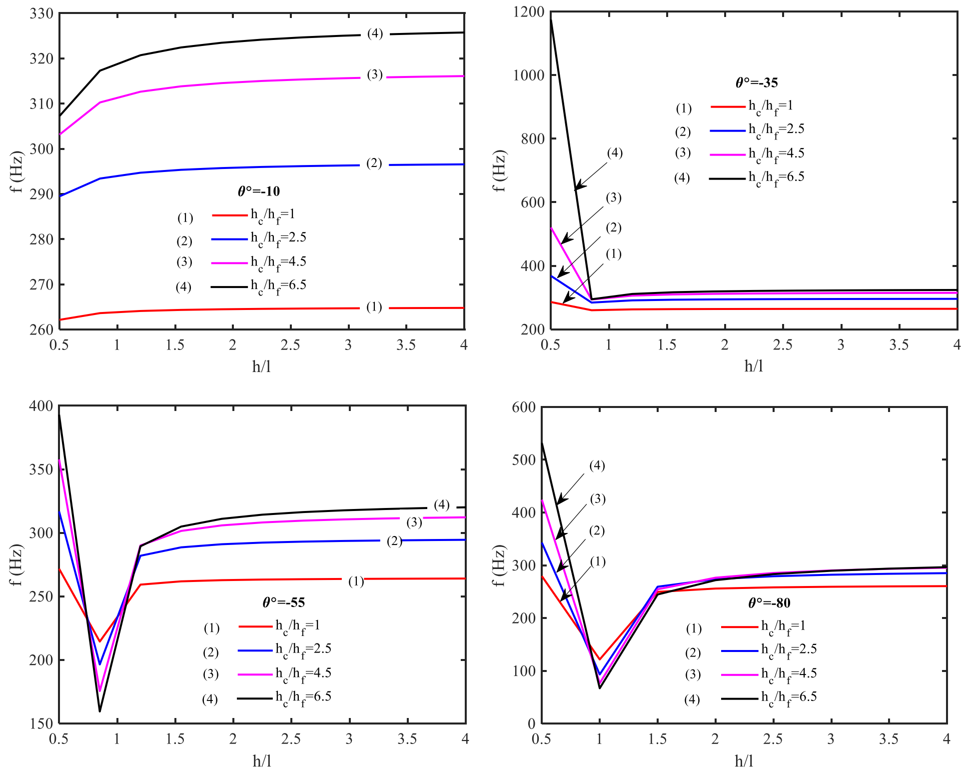


Figure 7. Variations of fundamental frequency $f$ (Hz) with $h/l$ ratio ($h_p = 0.1$ m, CCCC, $a = b = 20h_p, t/l = 0.1385$)

Variations of fundamental frequency $f$ (Hz) with $h/l$ ratio at different thickness ratios $h_c/h_f$ are shown in Fig. 7 for various inclined angle $\theta$ with clamped at all four edges. Again, the results showed irregularities of auxetic materials. With increasing the $h/l$ ratio, the natural frequencies of the plate with $\theta = -35°, -55°, -80°$ initially decrease while those of the plate with $\theta = -10°$ slightly increase at all $h_c/h_f$ values. It is further observed that the influence of the inclined angle $\theta$ on the natural frequency of the AHCL sandwich plate is more significant than that of the $h/l$ ratio.

b. Dynamic response of the AHCL sandwich plates

Next, analyses were performed to characterize the dynamic response of an AHCL sandwich plate to suddenly applied uniform pressure loading. The Newmark direct integration scheme [25] is used to reduce the semi-discrete finite element equations to fully discretized equations. A square simply supported AHCL sandwich plate with thickness $h_p = 0.1$ m under a suddenly applied uniform load $q_0 = -10^6$ N/m$^2$ is considered. The Rayleigh damping type is selected. In this damping model, damping matrix $\mathbf{C}_R$ is defined as a linear combination of mass and stiffness matrices which can be written as $\mathbf{C}_R = \alpha\mathbf{M} + \beta\mathbf{K}$. A timestep of $\Delta t = 10^{-5}$ s and the damping ratio $\xi = 0.8\%$ were used for all the cases.

Fig. 8 shows the effect of ratio $a/h = (10, 20, 30)$ on the dynamic response of the AHCL sandwich plate under suddenly applied uniform pressure loading. It is observed that the higher the $a/h$ ratio, the higher the amplitude of the plates. This reflects the fact that the higher the $a/h$ ratio, the thinner plate, which reduces the stiffness of the plate.

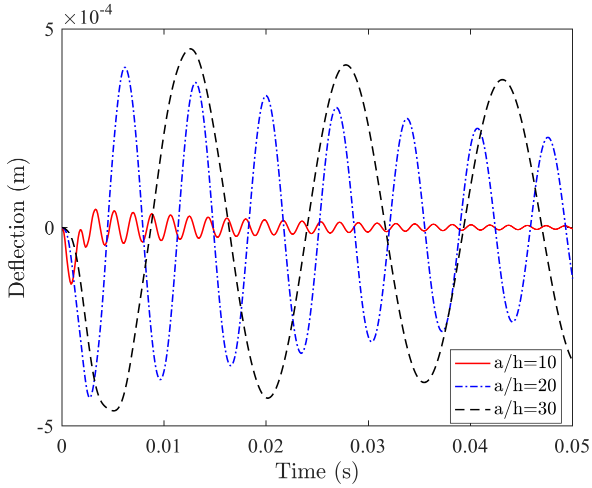


Figure 8. Center defection $w$ of AHCL sandwich plate at various thickness ratio $a/h$ (SSSS, $a = b, \theta = -50^\circ, h_c/h_f = 1.5, h/l = 2$)

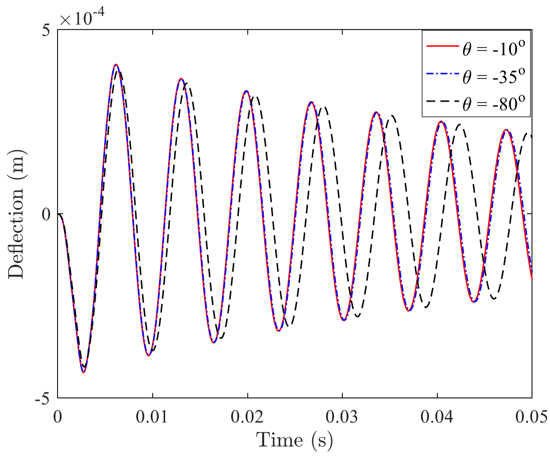


Figure 9. Center defection $w$ of the AHCL sandwich plate at various inclined angles $\theta$ (SSSS, $a = b, a/h = 20, h_c/h_f = 1.5, h/l = 2$)

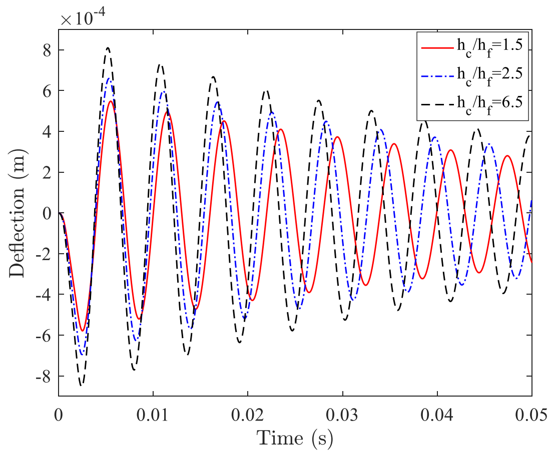


Figure 10. Center defection $w$ of the AHCL sandwich plate at different values of $h_c/h_f$ ratio (SSSS, $a = b, a/h = 20, \alpha = -50^\circ, h/l = 1$)

Fig. 9 illustrates the effect of the inclined angle $\theta$ on the amplitude–time curves of the AHCL sandwich plate. This figure shows that the plate with $\theta = -80^\circ$ vibrates with different frequencies and amplitude compared with other plates. This observation corresponds to the previous conclusion in the above section.

The influences of the $h_c/h_f$ ratio are shown in Fig. 10. It is seen that the amplitude of vibration increases smoothly as increasing of the $h_c/h_f$ ratio. This is because when the core layer thickness increases, the stiffness of the plate decreases, leading to an increase in deflection.

## 5. Conclusions

This study developed a cell-based smoothed discrete shear gap model based on the first-order shear deformation theory for the free vibration and dynamic analysis of the sandwich composite plate with the auxetic core. The accuracy and convergence of the model are validated through comparative examples. The influence of geometrical parameters, material properties, and boundary conditions on the dynamic responses and vibration of AHCL sandwich plates are computed. The results showed irregularities of auxetic materials. Unlike conventional materials, auxetic materials with negative Poisson coefficients have very unpredictable vibrational behavior. Conducted investigations show that by choosing the appropriate geometrical cell layout, it is possible to obtain desired mechanical behavior of the sandwich plate. Enhanced stiffness can be achieved for some particular combinations of geometrical cell units and geometrical plate parameters, thus increasing the structure's natural frequencies.

## References

[1] Scarpa, F., Tomlinson, G. (2000). Theoretical characteristics of the vibration of sandwich plates with in-plane negative Poisson's ratio values. *Journal of Sound and Vibration*, 230(1):45–67.

[2] Hadjigeorgiou, E. P., Stavroulakis, G. E. (2004). The use of auxetic materials in smart structures. *Computational Methods in Science and Technology*, 10(2):147–160.

[3] Ruzzene, M., Mazzarella, L., Tsopelas, P., Scarpa, F. (2002). Wave Propagation in Sandwich Plates with Periodic Auxetic Core. *Journal of Intelligent Material Systems and Structures*, 13(9):587–597.

[4] Strek, T., Jopek, H., Nienartowicz, M. (2015). Dynamic response of sandwich panels with auxetic cores. *Physica Status Solidi (b)*, 252(7):1540–1550.

[5] Mukhopadhyay, T., Adhikari, S. (2016). Free-Vibration Analysis of Sandwich Panels with Randomly Irregular Honeycomb Core. *Journal of Engineering Mechanics*, 142(11):06016008.

[6] Imbalzano, G., Tran, P., Ngo, T. D., Lee, P. V. S. (2016). A numerical study of auxetic composite panels under blast loadings. *Composite Structures*, 135:339–352.

[7] Zhang, Y., Li, X., Liu, S. (2016). Enhancing buckling capacity of a rectangular plate under uniaxial compression by utilizing an auxetic material. *Chinese Journal of Aeronautics*, 29(4):945–951.

[8] Duc, N. D., Seung-Eock, K., Tuan, N. D., Tran, P., Khoa, N. D. (2017). New approach to study nonlinear dynamic response and vibration of sandwich composite cylindrical panels with auxetic honeycomb core layer. *Aerospace Science and Technology*, 70:396–404.

[9] Novak, N., Starčevič, L., Vesenjak, M., Ren, Z. (2019). Blast response study of the sandwich composite panels with 3D chiral auxetic core. *Composite Structures*, 210:167–178.

[10] Cong, P. H., Long, P. T., Nhat, N. V., Duc, N. D. (2019). Geometrically nonlinear dynamic response of eccentrically stiffened circular cylindrical shells with negative poisson's ratio in auxetic honeycombs core layer. *International Journal of Mechanical Sciences*, 152:443–453.

[11] Li, C., Shen, H.-S., Wang, H. (2020). Postbuckling behavior of sandwich plates with functionally graded auxetic 3D lattice core. *Composite Structures*, 237:111894.

[12] Quan, T. Q., Anh, V. M., Mahesh, V., Duc, N. D. (2020). Vibration and nonlinear dynamic response of imperfect sandwich piezoelectric auxetic plate. *Mechanics of Advanced Materials and Structures*, 1–11.

[13] Nguyen, N. V., Nguyen-Xuan, H., Nguyen, T. N., Kang, J., Lee, J. (2021). A comprehensive analysis of auxetic honeycomb sandwich plates with graphene nanoplatelets reinforcement. *Composite Structures*, 259:113213.

[14] Reddy, J. N. (2006). *Theory and Analysis of Elastic Plates and Shells*. CRC Press.

[15] Reddy, J. N. (1984). A refined nonlinear theory of plates with transverse shear deformation. *International Journal of Solids and Structures*, 20(9-10):881–896.

[16] Quoc, T. H., Tu, T. M., Tham, V. V. (2019). Free Vibration Analysis of Smart Laminated Functionally Graded CNT Reinforced Composite Plates via New Four-Variable Refined Plate Theory. *Materials*, 12 (22):3675.

[17] Hanna, N. F., Leissa, A. W. (1994). A Higher Order Shear Deformation Theory for the Vibration of Thick Plates. *Journal of Sound and Vibration*, 170(4):545–555.

[18] Tham, V. V., Quoc, T. H., Tu, T. M. (2019). Free vibration analysis of smart laminated functionally graded carbon nanotube reinforced composite plates using four-variable refined plate theory. *Journal of Science and Technology in Civil Engineering (STCE) - HUCE*, 13(3V):42–54. (in Vietnamese).

[19] Zhu, P., Lei, Z. X., Liew, K. M. (2012). Static and free vibration analyses of carbon nanotube-reinforced composite plates using finite element method with first order shear deformation plate theory. *Composite Structures*, 94(4):1450–1460.

[20] Quoc, T. H., Huan, D. T., Tu, T. M., Tan, N. H. (2017). Bending analysis of functionally graded cylindrical shell panel under mechanical load and thermal effect-Analytical solution and Finite element model. *Journal of Science and Technology in Civil Engineering (STCE) - HUCE*, 11(2):38–46.

[21] Nguyen-Thoi, T., Phung-Van, P., Thai-Hoang, C., Nguyen-Xuan, H. (2013). A cell-based smoothed discrete shear gap method (CS-DSG3) using triangular elements for static and free vibration analyses of shell structures. *International Journal of Mechanical Sciences*, 74:32–45.

[22] Qing, T. D., Zhi, C. Y. *Wave propagation in sandwich panel with auxetic core*.

[23] Tran, T. T., Pham, Q. H., Nguyen-Thoi, T., Tran, T.-V. (2020). Dynamic Analysis of Sandwich Auxetic Honeycomb Plates Subjected to Moving Oscillator Load on Elastic Foundation. *Advances in Materials Science and Engineering*, 2020:1–16.

[24] Reddy, J. N. (2000). Analysis of functionally graded plates. *International Journal for Numerical Methods in Engineering*, 47(1-3):663–684.

[25] Newmark, N. M. (1959). A Method of Computation for Structural Dynamics. *Journal of the Engineering Mechanics Division*, 85(3):67–94.